Author Manuscript

Author Manuscript

Author Manuscript

Author Manuscript

HHS Public Access

Author manuscript

Brain Res. Author manuscript; available in PMC 2020 October 15.

Published in final edited form as:

Brain Res. 2019 October 15; 1721: 146327. doi:10.1016/j.brainres.2019.146327.

Over-expression of miR-34a induces rapid cognitive impairment and Alzheimer's disease-like pathology

S. Sarkar[a,d], **E.B. Engler-Chiurazzi**[a,d], **J.Z. Cavendis**[a,d], **J.M. Povroznik**[a,d], **A.E. Russell**[a,d], **D.D. Quintana**[a,d], **P.H. Mathers**[a,b], **J.W. Simpkins**[c,d,*]

[a]Department of Neuroscience, Rockefeller Neuroscience Institute, West Virginia University, Morgantown, WV 26506, United States

[b]Department of Biochemistry, Rockefeller Neuroscience Institute, West Virginia University, Morgantown, WV 26506, United States

[c]Department of Physiology & Pharmacology, Rockefeller Neuroscience Institute, West Virginia University, Morgantown, WV 26506, United States

[d]Center for Basic and Translational Stroke Research, Rockefeller Neuroscience Institute, West Virginia University, Morgantown, WV 26506, United States

Abstract

Autosomal dominant Alzheimer disease (AD) is caused by rare mutations in one of three specific genes. This is in contrast to idiopathic, late-onset AD (LOAD), which has a more polygenetic risk profile and represents more than 95% of cases. Previously, we have demonstrated that increased expression of microRNA (miRNA)-34a (miR-34a) in AD brain targets genes linked to synaptic plasticity, energy metabolism, and resting state network activity. Here we report the generation of a heterozygous, conditional miR-34a overexpression mouse (miR-34a$^{+/-}$(TetR-TetO-miR-34a) Transgenic Mice). Doxycycline-treated mice of either sex exhibited profound behavioral impairment compared to untreated groups with only 1–2 months of over-expression of miR-34a. Cognitive impairment of individual mice in T- and Y-maze tasks correlated with elevated miR-34a expression in many parts of the brain including the hippocampus and prefrontal cortex, regions which are known to be involved in this task and implicated in LOAD dysfunction. Immunocytochemistry of brain sections from mice show high amyloid β and phosphorylated tau-specific staining in the hippocampus and cortex. Analysis of protein samples from these mice revealed that miR-34a targets specific genes involved in memory formation, amyloid precursor protein (APP) metabolism and phosphorylation-dephosphorylation of tau. Thus, our results suggest that the polygenetic dysfunction caused by miR-34a may occur in LOAD and disclose miR-34a as a potential therapeutic target.

*Corresponding author at: 1 Medical Center Drive, West Virginia University, Morgantown, WV 26506, United States., jwsimpkins@hsc.wvu.edu (J.W. Simpkins).

Declaration of Competing Interest

The authors declare no conflicts of interest related to this research.

Author Manuscript Author Manuscript Author Manuscript Author Manuscript

Keywords

Late-onset Alzheimer's disease; microRNA; miR-34a; β amyloid; Tau phosphorylation; Memory-related behaviors; NMDAR 2B; SIRT1; ADAM10

1. Introduction

LOAD accounts for more than 95% of AD cases, making it the most common form of dementia (Querfurth and LaFerla, 2010). Yet currently, there are no effective treatments. Recently, genome-wide association studies (GWAS) of AD have identified dozens of novel risk factor genes (Seshadri et al., 2010), and their deregulated expression may be involved in AD pathogenesis (Allen et al., 2012). Furthermore, genome-wide transcriptome studies indicate that many important genes necessary for energy metabolism and synapse activity are downregulated in AD (Liang et al., 2008). Thus, polygenetic risk factors and reduced expression of many genes in LOAD impedes the path to progress in generating a useful mouse model and success for identifying novel target(s) for disease-modifying therapies.

The approach we took to model polygenetic AD risk factors is the generation of a mouse model using Tet-on/off switching-based expression of a pathogenic micro-RNA (miRNA), miR-34a, in adult mice that has the potential to induce a LOAD phenotype. Recent evidence suggests that several miRNAs are closely correlated with AD pathology by mechanisms such as regulation of the production of Aβ and phosphorylation of tau and inflammatory responses (Hebert et al., 2008; Kim et al., 2015; Smith et al., 2011; Vilardo et al., 2010). Among these miRNAs, miR-34a is upregulated in the hippocampus, medial frontal gyrus, and cerebellum of AD subjects (Cogswell et al., 2008), and clinical studies suggest that plasma miR-34a-5p and miR-545–3p may be early biomarkers of AD (Cosín-Tomás et al., 2017). Our previous investigation suggested that increased expression of miR-34a in brains of AD patients correlated with the severity of AD pathology, which may be partially due to the concomitant polygenic repression of synaptic plasticity, oxidative phosphorylation, and glycolysis-related genes (Sarkar et al., 2016). Further, our *in silico* analysis of human genomic sequences from the putative promoter of the miR-34a gene showed the presence of NFκB1, STAT1, c-Fos, CREB and p53 response elements (Sarkar et al., 2016). Activation of these transcription factors due to brain inflammation, metabolic and/or oxidative stresses, as well as excessive neural activity that occurs during aging, may lead to increased miR-34a gene expression and ultimately drive AD progression.

At present, the role of miR-34a in regulating AD pathology and impairing cognitive function has not been described. In this study, we have generated conditional miR-34a over-expressing mice and investigated the functional consequences of polygenic suppression of miR-34a target genes by identifying shared behavioral and molecular signatures characteristics of LOAD in the human.

Author Manuscript Author Manuscript Author Manuscript Author Manuscript

2. Methods

2.1. Generation of the animal model

Mouse lines were generated by the following sequential steps including 1) cloning miR-34a gene ahead of a promoter containing tetracycline response element plasmid (PmRi-mCherry); 2) co-injecting the purified insert into the pronucleus of FVB mouse zygotes along with the Tet repressor expression fragment (pTet-On Advanced) to achieve inducibility of the miR-34a expression in response to Doxy exposure; 3) implantation of the injected zygotes into pseudopregnant mice, 4) genotyping of the offspring by a PCR-based genotyping of tail biopsied DNA, as well as microscopic identification of mCherry-positive skin cells cultured from the tail biopsy, to identify transgenic founders, and 5) breeding of founders to produce required numbers of miR-34a$^{+/-}$ mice for the experiments.

2.2. Behavioral testing

Behavioral tests included in the test battery are described in the order in which they were conducted. All animals underwent all the tests, administered by a pair of experimenters who were blinded to treatments the animals received. All testing occurred under ambient lighting, unless otherwise noted. Between each animal, each apparatus was cleaned of debris and olfactory cues using an anti-bacterial disinfectant (Virkon, Pharmacol, CT).

2.2.1. Open field test—This task evaluates locomotor activity and "emotional" reactivity (Denenberg, 1969). Total movement in the arena indicates general locomotor ability and movement in the center vs periphery/corners indicates anxiety status. The apparatus consisted of a clear plastic box (40 cm × 40 cm) surrounded by a 16 × 16 laser beam array (San Diego Instruments, CA) that allowed for the assessment of movement in the horizontal axis. A second array placed 3.8 cm above the first beam allowed for the assessment of locomotion in the vertical axis (rearing behavior). Locomotor activity (measured as fine or ambulatory movements) was recorded using the Photobeam Activity System (San Diego Instruments). Following a 30-minute acclimation to the testing room (approximately 1500 lx), each subject was placed in the center point of the arena and allowed to freely explore for 30 min. To assess treatment-induced alterations in anxiety-like behavior, the open field arena was divided into a central square zone (approximately 700 cm^2) and a peripheral frame (approximately 940 cm^2) zone and horizontal locomotion was assessed in each zone (peripheral, central, and arena). Thus, dependent variables were the number of horizontal movements via beam breaks (fine and ambulatory combined) in the arena as well as in the peripheral and central zones, and the number of vertical beam breaks (rearing).

2.2.2. Accelerating rotarod—To evaluate locomotor learning as we have done previously (Doll et al., 2015), coordination and balance under conditions of increasing demand, mice were placed on a rotating beam set initially to 4 rpm. Once all mice were placed on the beam and stable in their movement (approx. 10 sec), the speed of rotation was increased progressively during a trial (4–40 RPM over 5 min) and the latency to fall from the beam was recorded. Mice received three trials with an intertrial interval of 10–15 min.

Author Manuscript Author Manuscript Author Manuscript Author Manuscript

2.2.3. Hot plate—This test assesses nociceptive ability in rodents in response to a thermal noxious stimulus (Bannon and Malmberg, 2007). For this test, the hot plate apparatus (Model 39; IITC, CA) was set to 55.0 °C. A single subject was placed onto the hot plate surface and confined using a square plastic enclosure. The total duration of hot plate exposure was 30 s. The dependent variable, latency (s) to first nociceptive behavior, defined as flicking/shaking, licking of a hindlimb or jumping (all four paws cease contact with the heated surface), was recorded. Type of nociceptive behavior was also documented. As well, the number of nociceptive behaviors of each subtype (hindlimb flicks, hindlimb licks or jumps) and the total number of observed nociceptive behaviors were documented.

2.2.4. Y-maze spontaneous alternation—In this land-based test of short-term memory, after a 30-minute room acclimation period, under indirect dim illumination conditions (approximately 150 lx), mice were placed in the three-armed, Y-shaped apparatus (approximate arm length = 38 cm, width = 8.25 cm, height = 13.25 cm) and allowed to freely explore for 8 min. Movement in the apparatus was recorded using the Anymaze tracking software (Stoelting, Chicago, IL). The innate tendency of mice to spontaneously alternate between the three arms and enter the least recently visited arm was assessed by determining the percent of successful alternations ((number of correct alternations/(total arm entries − 2)*100). Spatial cues (pictures of dark geometric basic shapes contrasting a white background) were present to aid in navigation/arm discrimination. Other dependent variables recorded included distance moved (m) and speed (m/s).

2.2.5. T-maze forced alternation—This land-based, forced win-shift test of hippocampal-dependent working and reference memory requires mice to alternate between spatial locations to earn reward. Under indirect dim illumination conditions (approximately 50 lx), animals were tested in a T-shaped apparatus (approximate arm length = 40 cm and 62.25 cm, width = 8.25 cm, height = 8.25 cm). For a given test day, animals were tested on 1 trial pair/day in which an animal was placed in the maze at the end of one of the arms and allowed to freely explore. In a given trial pair, for trial 1 (sample trial), one of the arms was blocked such that only two arms were accessible. For the second trial (test trial), all arms were made accessible. To successfully complete the task, the animal must shift to the previously inaccessible arm to obtain maze-escape, hence requiring working memory. For a given animal, the rewarded sequence of turn directions was held constant across all days, allowing reference memory learning over time to be assessed. Mice were tested daily for 6 days. Movement in the apparatus was recorded using the Anymaze tracking software (Stoelting, Chicago, IL) and test trial errors (entries into the accessible arm on the sample trial) were scored by an observer. Spatial cues were present to aid in navigation. Arm entries, as well as distance moved (m) and speed (m/s) were the dependent variables.

2.3. Tissue collection

Animals were euthanized in accordance with American Veterinary Association guidelines using isoflurane inhalation followed by decapitation. Tissues collected included the entorhinal cortex (EC), hippocampus (HI), prefrontal cortex (PFC) and the thalamus (TH); all tissues were frozen on dry ice and then stored at − 80 °C until further processing. Tissues from a randomly selected subset of behaviorally characterized mice from each treatment

Author Manuscript Author Manuscript Author Manuscript Author Manuscript

group were used for western blot and immunohistochemistry analyses of dependent measures of interest.

2.4. Immunohistochemistry and western blot

For immunohistochemistry, mice were killed at 2 months of Doxy (or no doxy treatment), and frozen sections (50 μm) of whole brain slices were made for the entorhinal cortex, hippocampus, prefrontal cortex and the thalamus. In brief: Transcranial 4% paraformaldehyde-perfused mice brains after cryoprotection in 30% sucrose were cryosectioned with a vibratome at a thickness of 50 μm. To expose target proteins in the paraformaldehyde fixed tissue sections, antigen retrieval were performed using 10 mM sodium citrate (pH 6.0), at 95 °C air oven for 20 min. Following antigen retrieval, tissues were blocked in 3% HR_2ROR_2R-methanol for 15 min at room temperature, washed with $ddHR_2RO$ and phosphate-buffered saline pH7.2 (PBS), and then probed with a specific antibody diluted in 3% BSA-PBS at a dilution of 1:250 and incubating overnight at 4 °C in a humidified chamber. The antibodies used were, Phospho-specfic tau (pSer202/pThr205 Tau antibody (AT8), clone MN1020 (Thermo Scientific, 0.2mg/ml stock concentration) and Antiβ-Amyloid Antibody clone 6E10, (Bio Legend, 1 mg/ml). Tissues were washed extensively in PBS, and detection was performed using an HRP-conjugated secondary antibody followed by colorimetric detection using a DAB peroxidase substrate kit (SK-4100, Vector Lab) according to suppliers' protocol.

For western blot analysis, tissue from the EC, PFC, HI and TH were homogenized in RIPA lysis buffer with addition of protease inhibitors cocktail (Sigma, St. Louis, MO, USA), followed by centrifugation at 13,400*g* for 5 min at room temperature (RT). The supernatants were collected and protein samples separated by electrophoresis run on a precast SDS-PAGE Mini-PROTEANT GX Gels 4–20% (Bio-Rad Laboratories). Equal protein levels were loaded in each well, with the protein concentration determined by a Bradford assay kit (Bio-Rad). After gel electrophoresis, the proteins were transferred onto PVDF membranes Immobilion (EMD Millipore). The respective membranes were then immunoprobed with the following primary antibodies: Tau (A-10) mouse monoclonal antibody for total Tau, (Santa Cruz Biotechnology, 250 μg/ml); Phospho-specfic tau (pSer202/pThr205) Tau antibody (AT8), clone MN1020 (Thermo Scientific, 0.2 mg/ml); Tau (Tau46) detects pSer 396 (Cell Signaling, 643 μg/ml), anti-ADAM10 antibody rabbit monoclonal (ABCAM, 1 mg/ml), SIRT1, Mouse monoclonal (Cell Signaling, 116 μg/ml), mouse monoclonal NMDAR2B (GRIN2B) antibody (BD Transduction Laboratory, 250 μg/ ml), and anti-PTPA mouse monoclonal antibody (ABCAM, 480 μg/ml). After overnight incubation with primary antibodies (1:1000 dilution), the membranes were washed and followed by incubation at room temperature for 2 h. with appropriate anti-rabbit or anti-mouse, secondary antibody conjugated with IR Dye (LI-COR). After washing, the specific reaction blots were visualized and photographed by using Near-Infrared western blots image acquiring system ODYSSEY CLX (LI-COR). After the antibodies were stripped by incubating the membranes at 50 °C for 30 min in stripping buffer composed of 62.5 mM Tris-HCl, pH 6.7, 2%SDS and 100 mM 2-mercaptoethanol, they were processed for relabeling with antibody against actin or GAPDH protein (C2, Santa Cruz Biotechnologies) or non-phospho tau

Author Manuscript Author Manuscript Author Manuscript Author Manuscript

(total) protein in case of p-tau internal control. Immunoblot bands were quantified by densitometry using ODYSSEY software (LI-COR).

2.5. Statistical analysis of data

Behavior and western blot densitometric data (Mean ± SEM) were analyzed with Student's *t*-test with Treatment (No Doxy or Doxy administration) as the independent factor or two-way ANOVA, with Treatment as the between factor and Brain Region (EC, HI, PFC, or TH) as the repeated factor, as appropriate for each given dependent measure using Prism 7 (GraphPad, San Diego, CA). Significant higher order interactions or main effects were followed by Bonferroni-corrected multiple comparison tests. Group differences were considered statistically significant when $p < 0.05$.

3. Results

3.1. Performance of miR-34a + / − mice in Y-maze and T-maze cognitive tasks

In its early stages, AD is characterized by several types of explicit memory impairment, such as deficits in episodic memory, semantic memory and working memory, whereas other types of memory such as implicit or procedural memory are relatively preserved until late in the disease process (Carlesimo and Oscar-Berman, 1992). Working memory is perhaps one of the most well modeled aspects of the memory deficits in AD. Clinically, many of the neuropsychological tests that assess working memory rely heavily on the use of verbal tasks (Benedict and Groninger, 1995; Benedict et al., 1998), employing language as a core construct and thus are not feasible to model using mice. Instead, hippocampal-dependent, spatial-based working memory tasks are heavily employed in murine working memory testing and likely are more depictive of the visuospatial working memory tasks used clinically. The most widely used paradigms for working memory in mice are T- or Y-maze type tasks, which require spatial working memory to solve.

Accordingly, we used a doxycycline (doxy)-induced conditional miR-34a over-expression mouse line (miR-34a + /− (TetR-TetO-miR34a)) to assess the effects of miR-34a over-expression on their performances in the spontaneous alternation Y-maze and forced alternation T-maze cognitive tasks. Mouse lines were generated as described in the methods section and in Fig. 1. At 4–5.5 months of age, mice were exposed to doxy (or no doxy) drinking water (2 mg/ml). Mice were assessed for health and sickness behavior for 4 weeks. The health and sickness behavior screen was performed as described previously (Doll et al., 2015) at baseline and twice per week for four weeks. Composite health scores averaged 0.3 out of 20 for both groups indicating minimal sickness. No difference in temperature, respiration rate, body condition, hydration, appearance, posture, or locomotion were observed. Mice gained an average of 9 (±7) percent body weight with no differences in weight gain between doxy- and vehicle-treated groups. Soon thereafter, mice were evaluated for reflexive and motor capabilities, as well as differences of anxiety-like behaviors. Specifically, we used an open field test to measure locomotor and anxiety-like behaviors, a rotarod test for testing motor coordination and balance, and a hot plate test for evaluating thermal pain sensitivity. While some loco/sensorimotor effects of miR-34a over-expression were detected (Fig. 2), namely reduced overall movement in the Y-maze, open field and

Author Manuscript Author Manuscript Author Manuscript Author Manuscript

rotarod behavior were unaffected. Importantly, cognitive performance was measured using performance metrics normalized to locomotor activity, reducing the potential confounding impact of locomotor disruptions on the cognitive effects of miR-34a over-expression.

From 49 to 65 days of continuous vehicle or doxy exposure, male and female adult mice were evaluated for behavioral impacts of miR-34a overexpression in functional domains commonly reported to be disrupted with age. These mice demonstrated pronounced T-maze working/reference memory impairments and Y-maze spontaneous alternation deficits (Fig. 3). Among these doxy-treated mice, miR-34a levels were substantially increased in all brain regions assayed compared to vehicle-treated animals, including in HI and PFC, areas known to be involved in controlling working and reference memory (Table 1).

Preclinical research studies indicate that N-methyl-D-aspartate glutamate receptors (NMDA-Rs) are critically involved in working memory. For example, NMDA-Rs contribute to the recurrent cortical excitation that is thought to model the maintenance of information in working memory (Fellous and Sejnowski, 2003; Lisman et al., 1998; Seamans et al., 2003). In awake, behaving rodents, NMDA-R antagonists attenuate PFC neural activity associated with working memory maintenance, and NMDA-R antagonists impair working memory performance in both non-human primates and humans (Baron and Wenger, 2001; Ghoneim et al., 1985; Homayoun et al., 2004; Jackson et al., 2004; Krystal et al., 1994; Oye et al., 1992). It has been shown that treatment with the NMDARs antagonist, ketamine, to healthy human subjects while performing a spatial working memory task resulted in reduced accuracy on the task and PFC activation as measured by fMRI (Driesen et al., 2013). Also, NR2A-containing NMDARs in the PFC are required for working memory and that loss of NR2A predicts severity of age-related working memory impairment (McQuail et al., 2016). Moreover, the NMDARs antagonist, MK801, impairs working memory of mice performing Y-maze spontaneous alternation test (Suryavanshi et al., 2014). Although the precise mechanism by which miR-34a overexpression in PFC-hippocampal circuits impairs working memory is not clear, our *in silico* analysis (Table 2) suggests that miR-34a targets both human and mouse NR2A and NR2B mRNAs. Previously we demonstrated that increased expression of miR-34a in AD patient brains in the cortical regions correlate with the suppression of NR2A protein levels (Sarkar et al., 2016). In the present study, we analyzed the functional consequences of the miR-34a targets, NMDAR2B, in several the brain regions of doxy-treated mice. Western blot analysis showed that NR2B protein levels in the brain regions of doxy-treated mice were significantly reduced compared to vehicle-treated mice (Fig. 4A and B).

3.2. miR-34a targets genes involved in regulating APP metabolism, tau phosphorylation

Recent reports suggest that upregulation of miR-34a correlates with the aging process and neurodegeneration (Liu et al., 2012). Also, miR-34a expression is induced in the aging heart, and genetic deletion of miR-34a reduces age-associated cardiomyocyte cell death (Boon et al., 2013). Moreover, the longevity gene, SIRT1, plays an important role in normal and pathological aging. Loss of SIRT1 function causes impaired memory and synaptic plasticity by down regulating cyclic AMP response binding protein (CREB) and brain derived neurotrophic factor (BDNF) expression (Gao et al., 2010). Our search for predicted gene

Author Manuscript Author Manuscript Author Manuscript Author Manuscript

targets of miRNA-34a by Target Scan (www.targetscan.org; Argarwal, 2015) found (Table 2) both human and mouse SIRT1 mRNA are the targets of miR-34a, which has been confirmed experimentally (Yamakuchi et al., 2008). Since SIRT1 is necessary for cognitive function in mice (Gao et al., 2010; Michan et al., 2010), we measured SIRT1 protein levels in several brain regions of doxy-treated mice and compared these to protein samples from vehicle-treated transgenic mice. Indeed, SIRT1 protein levels were significantly reduced in the EC, HI, PFC, and TH regions from doxy-treated transgenic mice when compared with the same brain regions from vehicle-treated mice (Fig. 4C and D).

SIRT1 deletion enhances levels of acetylated-tau and pathogenic forms of p-tau *in vivo* (Min et al., 2010). As such, we next determined phosphorylation status of tau proteins in the same mouse brain protein samples. The western blot protein samples were probed with phospho-tau (amino acid residues S202, and S205) specific AT8 antibody, (Fig. 5A) and phospho-tau (amino acid residues S404, S409 and S422) tau46 antibody (Fig. 5C). The densitometric quantification of p-tau/ total tau protein level showed profound increases in p-tau in doxy-treated miR-34a mice (Fig. 5B and D). In addition, immunocytochemical analysis of brains from doxy-treated miR-34a mice using a p-tau specific AT8 antibody showed increased levels in hippocampal formation subregions (Fig. 5E). Thus, increased tau phosphorylation in brain regions that express increased miR-34a due to doxy-induction is implicated in AD tauopathy.

Although the exact mechanism by which miR34a over expressions increases tau-phosphorylation is not known, our miR-34a Target Scan analysis suggests that miR-34a targets both human and mouse protein phosphatase 2A activator, PTPA mRNA (also known as ppp2R4 gene; Table 2). Levels of PTPA proteins are decreased in the brains of AD patients and AD transgenic mouse models (Luo et al., 2013). Therefore, we determined PTPA protein levels in these same brain regions. In the western blot, protein samples were probed with PTPA-specific antibody (Fig. 6A). The densitometric quantification shows profound suppression in PTPA protein levels when normalized to GAPDH levels in doxy-treated miR-34a mice (Fig. 6B).

3.3. Detection of Ai pathology in doxycycline-induced miR-34a over-expressed mouse brains

SIRT1 attenuates amyloidogenic processing of APP in cell culture studies *in vitro* and transgenic mouse models of AD (Boon et al., 2013; Yamakuchi et al., 2008). Mechanistically, SIRT1 increases α-secretase production and activity through activation of the α-secretase gene, ADAM10 (Lee et al., 2014). Also, our Target Scan search revealed that miR-34a targets both human and mouse ADAM10 mRNA (Table 2), suggesting two potential mechanisms by which ADAM10 protein levels could be affected by miR-34a over-expression. We tested this possibility by western blot analysis of protein samples isolated from several brain regions by immunoblotting using ADAM10-specific antibody (Fig. 7A and B). Quantification of the western blot band by densitometry showed significant reduction of ADAM10 proteins in EC, HI, PFC, and TH brain regions in protein samples from doxy-treated compared to vehicle-treated mice. Inasmuch as ADAM10 suppression should drive APP processing toward Aβ formation, we next assessed using

Author Manuscript Author Manuscript Author Manuscript Author Manuscript

immunohistochemistry, Aβ in mice. Aβ-specific staining of EC (Fig. 7C) and HI (Fig. 7D) was much higher in miR34a$^{+/-}$ mice treated with doxy vs vehicle. The Aβ-specific staining appeared to be intracellular (Fig. 7E).

4. Discussion

The present study demonstrates the rapid onset of cognitive decline and AD neuropathology in mice in which miR-34a is over-expressed. The AD neuropathological features seen in these mice include 1) tau hyperphosphorylation, caused in part by a decline of the expression of the PP2A promoter, PTPA; 2) an accumulation of intraneuronal Aβ, associated with a marked decline in ADAM10; and 3) relative loss of NR2A, which is associated with cognitive decline and a decline in SIRT1, which itself may be involved in both the accumulation of Aβ and tau hyperphosphorylation. As such, we believe that over-expression of miR-34a causes neuropatholgical changes in the brain similar to those seen in human subjects with polygenetic risk factors for AD.

It has been reported that a decrease in α-secretase activity of ADAM10 and loss-of-function mutations of ADAM10 found in AD patient brains contributes to the generation of Ap and development of AD pathology, namely amyloid plaques (Suh et al., 2013). Over the past several years, the multifaceted deregulation of PP2A, including a significant decrease in total PP2A activity and down regulation of leucine carboxyl methyl transferase-1 and PTPA that correlate with enhanced tau phosphorylation, has been identified in AD brain tissues (Luo et al., 2013). Thus, severe reductions of SIRT1, ADAM10, and PTPA protein levels in miR-34a overexpressed brain regions could generate AD-like pathology, specifically increased Aβ and p-tau, and with extended doxy exposure possibly generating amyloid plaque and neurofibrillary tangles.

It is of interest that the miR-34a over-expression model causes a rapid appearance of cognitive decline and AD-like neuropathology. Indeed, the cognitive effects and AD neuropathology appear by 1–2 months of miR-34a over-expression, far sooner that these features are seen in single Tg AD mice (Carlson et al., 1997), 3×Tg AD mice (Oddo et al., 2003), and 5×Tg AD mice (Eimer and Vassar, 2013). As such, this mouse strain may be a useful model for the assessment of the earliest stages of AD neuropathology. Importantly, it is our observation that Aβ appears to be nearly exclusively intraneuronal at two months of over-expression of miR-34a, suggesting that the initial stages of Aβ neuropathology occur within neurons. Interestingly, intraneuronal Ap immunoreactivity is one of the earliest neuropathological manifestations in the 3×Tg-AD mice, first detectable at 3–4 months of age in neocortical regions and subsequently in CA1 pyramidal neurons, and by 6 months of age in the CA1 subfield of the hippocampus (Oddo et al., 2003). In the 3×Tg AD, extracellular Aβ deposits first became apparent in 8-month-old mice in the frontal cortex, predominantly in layers 4–5 and were readily evident by 12 months in both hemizygous and homozygous mice (Carlson et al., 1997).

An additional useful feature of this mouse model is our ability to turn on and turn off miR-34a at any life stage, allowing assessment of the interaction of age with miR-34a induced AD pathology. As well, this model provides the ability to assess the effects of

Author Manuscript Author Manuscript Author Manuscript Author Manuscript

transient induction of AD neuropathology (as opposed to genetically-driven constitutive expression) on the development, progression and persistence of AD symptoms. Indeed, whether Aβ plaques or tauopathy could spontaneously resolve once seeded, if the mechanism driving their development was halted, is not yet known and cannot be determined using currently available transgenic animal models. Determining the parameters that influence the induction and potential resolution of AD-associated neuropathological hallmarks following cessation of miR-34a overexpression could offer such important insights to the field. Further, this model may be useful for the assessment of neuroprotective or neurorestorative drug/nutrient interventions initiated before or after miR-34a over-expression.

Previously, we showed that associated with over-expression of the human AD brain, miR-34a targets genes linked to synaptic plasticity, energy metabolism, and resting state network activity (Sarkar et al., 2016. Also our analysis of human genomic sequences from the tentative promoter of miR-34a gene shows the presence of NFKB1, STAT1, c-Fos, CREB and p53 response elements. Oxidative stress activates p53 and neuroinflammation activates NFkB1 transcription factors. In human subjects, amplified neuroinflammatory responses following an immune challenge and chronic oxidative stress occur with normal aging (Fonken et al., 2016). Therefore, we reasoned that aging-induced activation of these transcription factors in the brain would induce miR-34a-mediated concurrent repression of its target genes in neuro-glia-vascular networks leading to a LOAD phenotype.

A dominant risk factor for LOAD is the epsilon-4 (e4) allele of apolipoprotein E (ApoE4), which is present in about two-thirds of patients. The ApoE4 allele confers increased risk for LOAD, but the precise molecular mechanisms underlying ApoE4-associated AD risk remain unclear. Recent studies shed light on a novel mechanism for ApoE4-mediated toxicity and revealed a key mediator, SIRT1 that is differentially affected by ApoE4 vs. ApoE3 (Theendakara et al., 2013). Our studies link miR-34a with one of the major longevity determinants, the SIRT1 gene, and like ApoE4, doxy-induced miR-34a expression in our transgenic mice brain also (i) reduces SIRT1 levels that could alter ratio of neuroprotective SIRT1 to neurotoxic SIRT2; (ii) reduces ADAM10 expression that in turn could reduce the ratio sAPPa to Aβ; and (iii) triggers tau phosphorylation.

SIRT1 also stimulates oxidative energy production via the activation of AMPK, PPAR-α, and PGC1-α and inhibits NFkB signaling directly by deacetylation of the p65 subunit of the NFkB1 complex (Canto and Auwerx, 2009; Yeung et al., 2004). Thus, inhibition of SIRT1 by miR-34a disrupts oxidative energy metabolism and stimulates NFkB-induced inflammatory responses, including miR-34a expression, perhaps resulting in a positive feedback enhancement of miR-34a expression. Also, it has been shown that miR-34c, another member of miR-34 family, targets SIRT1 and that intrahippocampal administration of antagomir miR-34c ameliorates learning impairment in a mouse model for AD (Zovoilis et al., 2011). As mentioned earlier, SIRT1 loss-of-function impairs memory and synaptic plasticity by down regulating expression of CREB and BDNF. In this study we have shown that miR-34a reduces NMDA-R 2B and it can also target NMDA-R 2A (not shown). NMDA-R 2B is involved in persistent neuronal firing during working memory in the prefrontal cortex (Wang et al., 2013). Increased miR-34a expression in the PFC of miR-34a

Author Manuscript Author Manuscript Author Manuscript Author Manuscript

mice correlates with poor working memory performance. Besides NMDAR-2B, BDNF also modulates cognitive function and facilitates long term potentiation (LTP). Importantly AD brains contain low levels of BDNF (Phillips et al., 1991) and consistently show synaptic loss (Selkoe, 2002).

The goal of our research project is to simulate human sporadic AD in animal model by examining at the molecular, cellular, and system level how polygenic dysfunctions cause initiation and/or progression of cognitive decline and dementia, including AD. AD pathology is linked to aging, the most important risk factor for AD. Aging is a complex process that is linked to an increased incidence of major diseases including cardiovascular and neurodegenerative diseases. Expression of miR-34a appear to be increased during cellular senescence, aging and cardiovascular and Alzheimer's disease. miR-34a targets up to hundreds of mRNAs, thereby modulating gene expression patterns. However, increased expression of miR-34a linked to dysfunctions in cardiac and brain functions has been established. Specifically, it has been shown that elevated miR-34a in the heart by targeting essential excitation-contraction coupler Junctophilin 2 (JPH2) (Hu et al., 2019), and the gene PNUTS (PPP1r10, protein phosphatase 1 regulator subunit 10.) dysregulates cardiac contractile function (Boon et al., 2013). Past studies suggests that dysfunctions in the vascular system-the heart and blood vessels that supply blood to the brain- can contribute to the development of dementia (Gottesman et al., 2017). Also, cardiac I_K1 and I_{KACh} are the major potassium currents displaying classical strong inward rectification, a unique property that is critical for their roles in cardiac excitability (Miake et al., 2003). Our in silico analysis revealed that miR34a targets Kir2.1 and Kir2.1 expression is severely reduced in brain regions where miR-34a is highly expressed. Because doxycycline induced miR-34a expression is not restricted to the brain in these mice, at present it cannot be decipher whether cognitive dysfunction seen in these mice are due to dysfunction of cardiovascular or neurovascular or both systems.

Hippocampal theta oscillations are continuously present during ongoing locomotion and represent a brain-state specialized for processing of spatially related input (Buzsaki, 2002). Also, before the onset of locomotion, the hippocampus undergoes a transition into an activity-state specialized for the processing of spatially related input. This brain-state transition is associated with increased firing rates of CA1 pyramidal neurons and the occurrence of theta oscillations, which both correlate with locomotion velocity (Arriaga and Han, 2017). Key regulators of locomotion-related theta oscillations are the medial septal nucleus and the diagonal band of Broca (MSDB). Septo-hippocampal projections might be crucially involved in the mechanisms by which CA1 pyramidal neurons increase their firing rates during locomotion (Fuhrmann et al., 2015). Thus low locomotor speed observed during Y-maze task performance in doxycycline-treated mice could affect cognitive performances by decreased firing rates of CA1 pyramidal neurons. Also, locomotion is a rhythmic and episodic behavior that is initiated and stopped according to behavioral needs. There is a possibility that miR-34a by inhibiting excitatory neurons in the lateral paragigantocellular nucleus (LPGi), a small subregion in the caudal brainstem, inhibits locomotor speed through inputs from glutamatergic neurons of the upstream midbrain locomotor region (Capelli et al., 2017).

Author Manuscript Author Manuscript Author Manuscript Author Manuscript

Tet on/off system is specifically designed for assessment of reversibility effects of transgene expression in mice. We are currently planning to test effects of time-dependent exposure of doxycycline in these mice. We expect that after transiently inducing miR-34a expression, its decline with withdrawal of doxycycline will ameliorate both pathology and cognitive function. Also, because analysis of degradation dynamics of mi-RNA revealed that majority of mi-RNA half-lives are $t_{½} > 24h$. (Marzi et al., 2016) and miRNA cannot inhibit transcription of genes that are needed for network activity involving cognitive functions, turning off of doxycycline treatment will reverse the miR-34a over-expressed phenotypes in these mice.

In conclusion, our results suggest that polygenetic dysfunction induced by miR-34a may occur in LOAD and disclose miR-34a as a potential therapeutic target.

Acknowledgement

This work was supported by NIH Grants P20 GM109098, P01 AG027956, T32 AG052375 and U54 GM10494243T.

References

Argarwal V, Bell GW, Nam J, Bartel DP, 2015 Predicting effective microRNA target sites in mammalian mRNAs.

Allen M, et al., 2012 Novel late-onset Alzheimer disease loci variants associate with brain gene expression. Neurology 79, 221–228. [PubMed: 22722634]

Arriaga M, Han EB, 2017 Dedicated hippocampal inhibitory networks for locomotion and immobility. J. Neurosci 37, 9222–9238. [PubMed: 28842418]

Bannon AW, Malmberg AB, 2007 Models of nociception: hot-plate, tail-flick, and formalin tests in rodents. Curr. Protoc. Neurosci 41, 8.9.1–8.9.16.

Baron SP, Wenger GR, 2001 Effects of drugs of abuse on response accuracy and bias under a delayed matching-to-sample procedure in squirrel monkeys. Behav. Pharmacol 12, 247–256. [PubMed: 11548110]

Benedict RHB, et al., 1998 Hopkins verbal learning test - revised: normative data and analysis of inter-form and test-retest reliability. Clin. Neuropsychol 12, 43–55.

Benedict RHB, Groninger L, 1995 Preliminary standardization of a new visuospatial memory test with six alternate forms. Clin. Neuropsychol 9, 11–16.

Boon RA, et al., 2013 MicroRNA-34a regulates cardiac ageing and function. Nature 495, 107–110. [PubMed: 23426265]

Buzsaki G, 2002 Theta oscillations in the hippocampus. Neuron 33, 325–340. [PubMed: 11832222]

Canto C, Auwerx J, 2009 PGC-1alpha, SIRT1 and AMPK, an energy sensing network that controls energy expenditure. Curr. Opin. Lipidol 20, 98–105. [PubMed: 19276888]

Capelli P, et al., 2017 Locomotor speed control circuits in the caudal brainstem. Nature 551, 373–377. [PubMed: 29059682]

Carlesimo GA, Oscar-Berman M, 1992 Memory deficits in Alzheimer's patients: a comprehensive review. Neuropsychol. Rev 3, 119–169. [PubMed: 1300219]

Carlson GA, et al., 1997 Genetic modification of the phenotypes produced by amyloid precursor protein overexpression in transgenic mice. Hum. Mol. Genet 6, 1951–1959. [PubMed: 9302276]

Cogswell JP, et al., 2008 Identification of miRNA changes in Alzheimer's disease brain and CSF yields putative biomarkers and insights into disease pathways. J. Alzheimers Dis 14, 27–41. [PubMed: 18525125]

Cosín-Tomás M, et al., 2017 Plasma miR-34a-5p and miR-545–3p as early biomarkers of Alzheimer's Disease: potential and limitations. Mol. Neurobiol 54, 5550–5562. [PubMed: 27631879]

Author Manuscript Author Manuscript Author Manuscript Author Manuscript

Denenberg VH, 1969 Open-field bheavior in the rat: what does it mean? Ann. N. Y. Acad. Sci 159, 852–859. [PubMed: 5260302]

Doll DN, et al., 2015 Lipopolysaccharide exacerbates infarct size and results in worsened post-stroke behavioral outcomes. Behav. Brain Funct 11, 32. [PubMed: 26463864]

Driesen NR, et al., 2013 The impact of NMDA receptor blockade on human working memory-related prefrontal function and connectivity. Neuropsychopharmacology 38, 2613–2622. [PubMed: 23856634]

Eimer WA, Vassar R, 2013 Neuron loss in the 5XFAD mouse model of Alzheimer's disease correlates with intraneuronal Abeta42 accumulation and Caspase-3 activation. Mol. Neurodegener 8, 2. [PubMed: 23316765]

Fellous JM, Sejnowski TJ, 2003 Regulation of persistent activity by background inhibition in an in vitro model of a cortical microcircuit. Cereb. Cortex 13, 1232–1241. [PubMed: 14576214]

Fonken LK, et al., 2016 The alarmin HMGB1 mediates age-induced neuroinflammatory priming. J. Neurosci 36, 7946–7956. [PubMed: 27466339]

Fuhrmann F, et al., 2015 Locomotion, theta oscillations, and the speed-correlated firing of hippocampal neurons are controlled by a medial septal glutamatergic circuit. Neuron 86, 1253–1264. [PubMed: 25982367]

Gao J, et al., 2010 A novel pathway regulates memory and plasticity via SIRT1 and miR-134. Nature 466, 1105–1109. [PubMed: 20622856]

Ghoneim MM, et al., 1985 Ketamine: behavioral effects of subanesthetic doses. J. Clin. Psychopharmacol 5, 70–77. [PubMed: 3988972]

Gottesman RF, et al., 2017 Associations between midlife vascular risk factors and 25-year incident dementia in the atherosclerosis risk in communities (ARIC) cohort. JAMA Neurol. 74, 1246–1254. [PubMed: 28783817]

Hebert SS, et al., 2008 Loss of microRNA cluster miR-29a/b-1 in sporadic Alzheimer's disease correlates with increased BACE1/beta-secretase expression. Proc. Natl. Acad. Sci. U.S.A 105, 6415–6420. [PubMed: 18434550]

Homayoun H, et al., 2004 Functional interaction between NMDA and mGlu5 receptors: effects on working memory, instrumental learning, motor behaviors, and dopamine release. Neuropsychopharmacology 29, 1259–1269. [PubMed: 15010696]

Hu J, et al., 2019 RBFox2-miR-34a-Jph2 axis contributes to cardiac decompensation during heart failure. Proc. Natl. Acad. Sci. U.S.A 116, 6172–6180. [PubMed: 30867288]

Jackson ME, Homayoun H, Moghaddam B, 2004 NMDA receptor hypofunction produces concomitant firing rate potentiation and burst activity reduction in the prefrontal cortex. Proc. Natl. Acad. Sci. U.S.A 101, 8467–8472. [PubMed: 15159546]

Kim J, et al., 2015 microRNA-33 regulates ApoE lipidation and amyloid-beta metabolism in the brain. J. Neurosci 35, 14717–14726. [PubMed: 26538644]

Krystal JH, et al., 1994 Subanesthetic effects of the noncompetitive NMDA antagonist, ketamine, in humans. Psychotomimetic, perceptual, cognitive, and neuroendocrine responses. Arch. Gen. Psychiatry 51, 199–214. [PubMed: 8122957]

Lee HR, et al., 2014 Cilostazol suppresses beta-amyloid production by activating a disintegrin and metalloproteinase 10 via the upregulation of SIRT1-coupled retinoic acid receptor-beta. J. Neurosci. Res 92, 1581–1590. [PubMed: 24903973]

Liang WS, et al., 2008 Alzheimer's disease is associated with reduced expression of energy metabolism genes in posterior cingulate neurons. Proc. Natl. Acad. Sci. U.S.A 105, 4441–4446. [PubMed: 18332434]

Lisman JE, Fellous JM, Wang XJ, 1998 A role for NMDA-receptor channels in working memory. Nat. Neurosci 1, 273–275. [PubMed: 10195158]

Liu N, et al., 2012 The microRNA miR-34 modulates ageing and neurodegeneration in Drosophila. Nature 482, 519–523. [PubMed: 22343898]

Luo Y, et al., 2013 PTPA activates protein phosphatase-2A through reducing its phosphorylation at tyrosine-307 with upregulation of protein tyrosine phosphatase 1B. Biochim. Biophys. Acta 1833, 1235–1243. [PubMed: 23428800]

Author Manuscript Author Manuscript Author Manuscript Author Manuscript

Marzi MJ, et al., 2016 Degradation dynamics of microRNAs revealed by a novel pulse-chase approach. Genome Res. 26, 554–565. [PubMed: 26821571]

McQuail JA, et al., 2016 NR2A-containing NMDARs in the prefrontal cortex are required for working memory and associated with age-related cognitive decline. J. Neurosci 36, 12537–12548. [PubMed: 27807032]

Miake J, Marban E, Nuss HB, 2003 Functional role of inward rectifier current in heart probed by Kir2.1 overexpression and dominant-negative suppression. J. Clin. Invest 111, 1529–1536. [PubMed: 12750402]

Michan S, et al., 2010 SIRT1 is essential for normal cognitive function and synaptic plasticity. J. Neurosci 30, 9695–9707. [PubMed: 20660252]

Min SW, et al., 2010 Acetylation of tau inhibits its degradation and contributes to tauopathy. Neuron 67, 953–966. [PubMed: 20869593]

Oddo S, et al., 2003 Triple-transgenic model of Alzheimer's disease with plaques and tangles: intracellular Abeta and synaptic dysfunction. Neuron 39, 409–421. [PubMed: 12895417]

Oye I, Paulsen O, Maurset A, 1992 Effects of ketamine on sensory perception: evidence for a role of N-methyl-D-aspartate receptors. J. Pharmacol. Exp. Ther 260, 1209–1213. [PubMed: 1312163]

Phillips HS, et al., 1991 BDNF mRNA is decreased in the hippocampus of individuals with Alzheimer's disease. Neuron 7, 695–702. [PubMed: 1742020]

Querfurth HW, LaFerla FM, 2010 Alzheimer's disease. N. Engl. J. Med 362, 329–344. [PubMed: 20107219]

Sarkar S, et al., 2016 Expression of microRNA-34a in Alzheimer's disease brain targets genes linked to synaptic plasticity, energy metabolism, and resting state network activity. Brain Res. 1646, 139–151. [PubMed: 27235866]

Seamans JK, Nogueira L, Lavin A, 2003 Synaptic basis of persistent activity in prefrontal cortex in vivo and in organotypic cultures. Cereb. Cortex 13, 1242–1250. [PubMed: 14576215]

Selkoe DJ, 2002 Alzheimer's disease is a synaptic failure. Science 298, 789–791. [PubMed: 12399581]

Seshadri S, et al., 2010 Genome-wide analysis of genetic loci associated with Alzheimer disease. JAMA 303, 1832–1840. [PubMed: 20460622]

Smith P, et al., 2011 In vivo regulation of amyloid precursor protein neuronal splicing by microRNAs. J. Neurochem 116, 240–247. [PubMed: 21062284]

Suh J, et al., 2013 ADAM10 missense mutations potentiate beta-amyloid accumulation by impairing prodomain chaperone function. Neuron 80, 385–401. [PubMed: 24055016]

Suryavanshi PS, et al., 2014 GluN2C/GluN2D subunit-selective NMDA receptor potentiator CIQ reverses MK-801-induced impairment in prepulse inhibition and working memory in Y-maze test in mice. Br. J. Pharmacol 171, 799–809. [PubMed: 24236947]

Theendakara V, et al., 2013 Neuroprotective Sirtuin ratio reversed by ApoE4. Proc. Natl. Acad. Sci. U.S.A 110, 18303–18308. [PubMed: 24145446]

Vilardo E, et al., 2010 MicroRNA-101 regulates amyloid precursor protein expression in hippocampal neurons. J. Biol. Chem 285, 18344–18351. [PubMed: 20395292]

Wang M, et al., 2013 NMDA receptors subserve persistent neuronal firing during working memory in dorsolateral prefrontal cortex. Neuron 77, 736–749. [PubMed: 23439125]

Yamakuchi M, Ferlito M, Lowenstein CJ, 2008 miR-34a repression of SIRT1 regulates apoptosis. Proc. Natl. Acad. Sci. U.S.A 105, 13421–13426. [PubMed: 18755897]

Yeung F, et al., 2004 Modulation of NF-kappaB-dependent transcription and cell survival by the SIRT1 deacetylase. EMBO J. 23, 2369–2380. [PubMed: 15152190]

Zovoilis A, et al., 2011 microRNA-34c is a novel target to treat dementias. EMBO J. 30, 4299–4308. [PubMed: 21946562]

Author Manuscript Author Manuscript Author Manuscript Author Manuscript

HIGHLIGHTS

- Sporadic Alzheimer's disease (sAD) is difficult to model in animals.
- We produced a conditional over-expressing, miR-34a mouse to model sAD.
- miR-34a over-expression results in a rapid cognitive impairment.
- miR-34a over-expression also induces AD pathology in various cognitive brain regions.
- Inducible miR-34a mice may represent a polygenetic risk factor model for sAD.

Author Manuscript Author Manuscript Author Manuscript Author Manuscript

Significance Statement:

Late-onset Alzheimer disease (LOAD) is associated with multiple gene alleles, a polygenetic profile of risk factors that is difficult to model in animals. Our approach to modeling LOAD was to produce a conditional over-expressing, miR-34a mouse using doxycycline-induction to activate expression. We observed that miR-34a over-expression results in a rapid cognitive impairment, associated with accumulation of intracellular Aβ and tau hyperphosphorylation in multiple brain regions. Targets for miR-34a, including ADAM10, NMDAR 2B, and SIRT1 RNAs, were profoundly reduced by miR-34a over-expression. Collectively, these results indicate that a rapid, profound cognitive decline and Alzheimer's disease neuropathology can be induced with miR-34a over-expression, suggesting that this animal model may represent a polygenetic risk factor model for LOAD.

Author Manuscript Author Manuscript Author Manuscript Author Manuscript

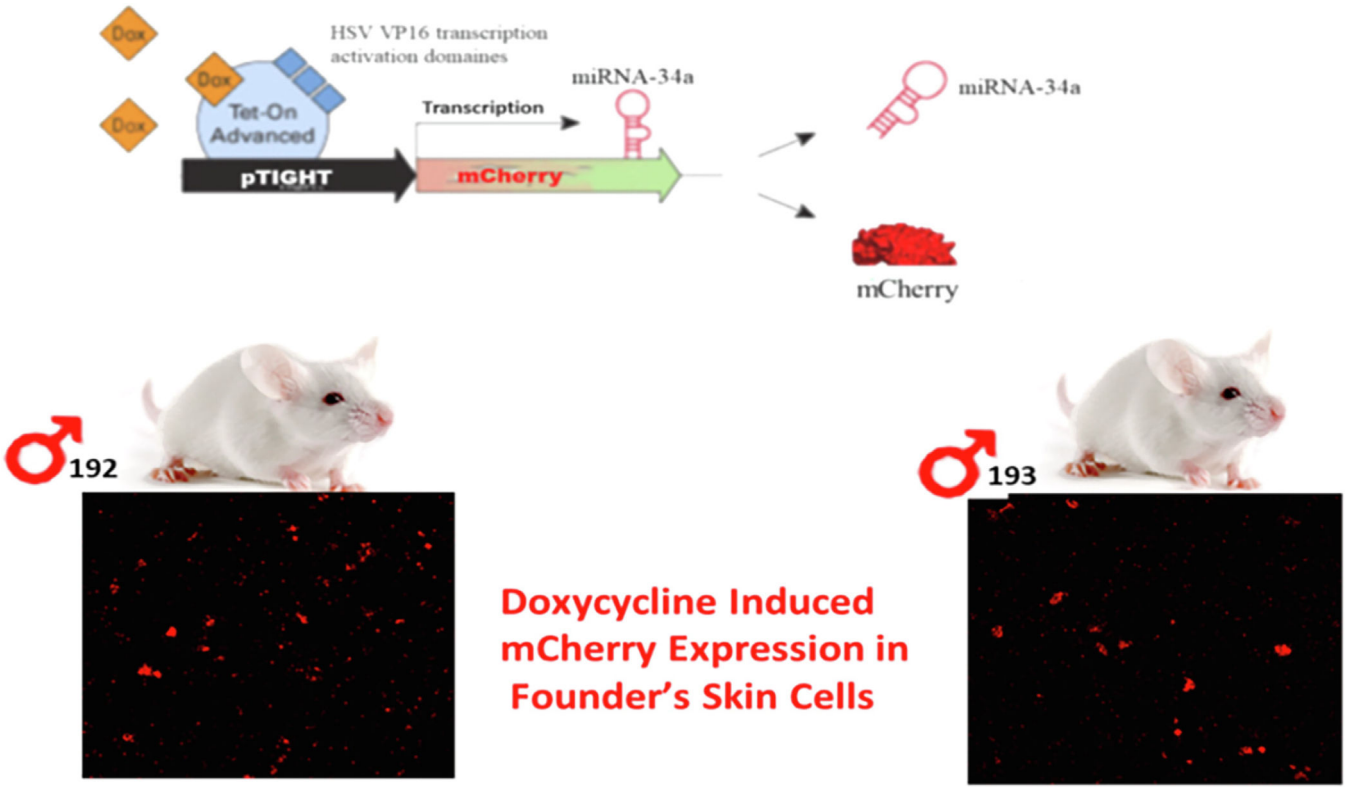

Fig. 1.

Generation of transgenic mice. The mouse lines were generated cloning miR-34a gene ahead of a promoter containing tetracycline response element plasmid (PmRi-mCherry). This construct was injected into the pronucleus of mouse zygotes along with the Tet repressor expression plasmid (pTet-On Advanced) to achieve inducibility of the miR-34a expression in response to Doxy exposure. The correct genotype of offspring was verified by PCR-based genotyping of tail biopsied DNA as well as microscopic identification of red colored m-cherry positive expression in their respective skin cells.

Author Manuscript Author Manuscript Author Manuscript Author Manuscript

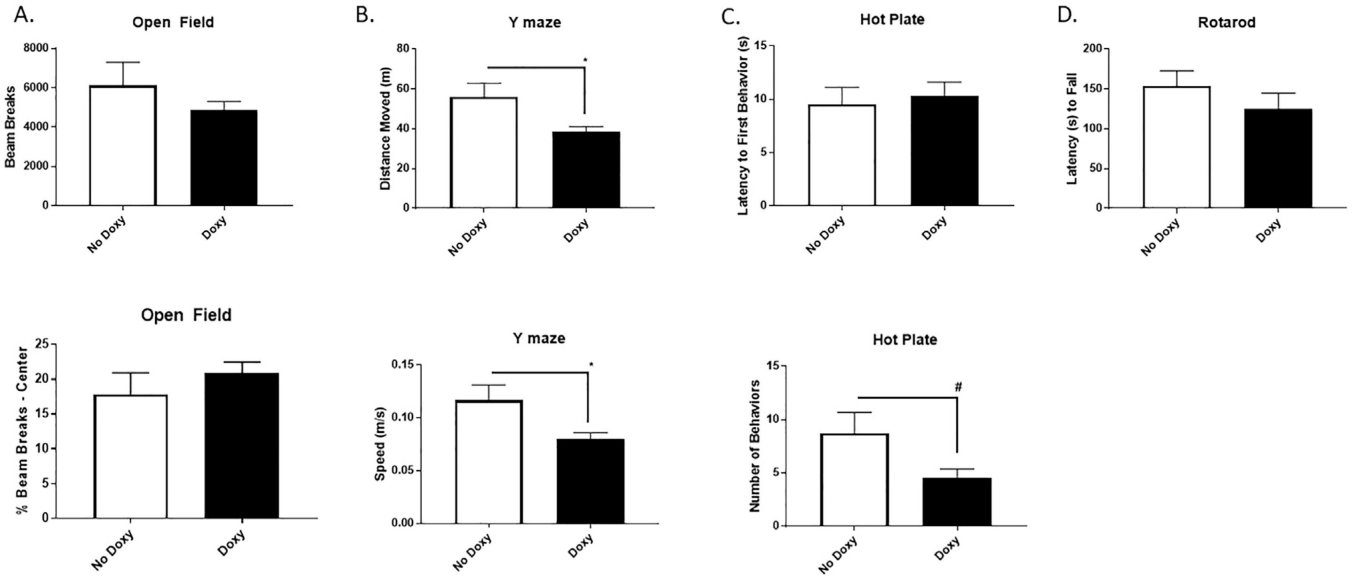

Fig. 2.

Locomotor and behavioral phenotyping of transgenic mice with or without doxy exposure. A. Doxy exposure had no impact on either open field spontaneous locomotion (upper panel) or anxiety-like behavior (lower panel). B. Y-maze total distance moved [$t(13) = 2.47$, $p < 0.05$] (upper panel) and speed [$t(13) = 2.47$, $p < 0.05$] (lower panel) were reduced among mice given Doxy vs No Doxy controls. C. Hot plate total nociceptive behaviors (lower panel) tended to be reduced among mice given Doxy vs No Doxy controls [$t(13) = 2.06$, $p < 0.07$] but latency to first nociceptive behavior (upper panel) was not altered between the groups. D. Rotarod coordination was not different between the groups. * $p < 0.05$. $N = 7–8$ mice/group.

Author Manuscript Author Manuscript Author Manuscript Author Manuscript

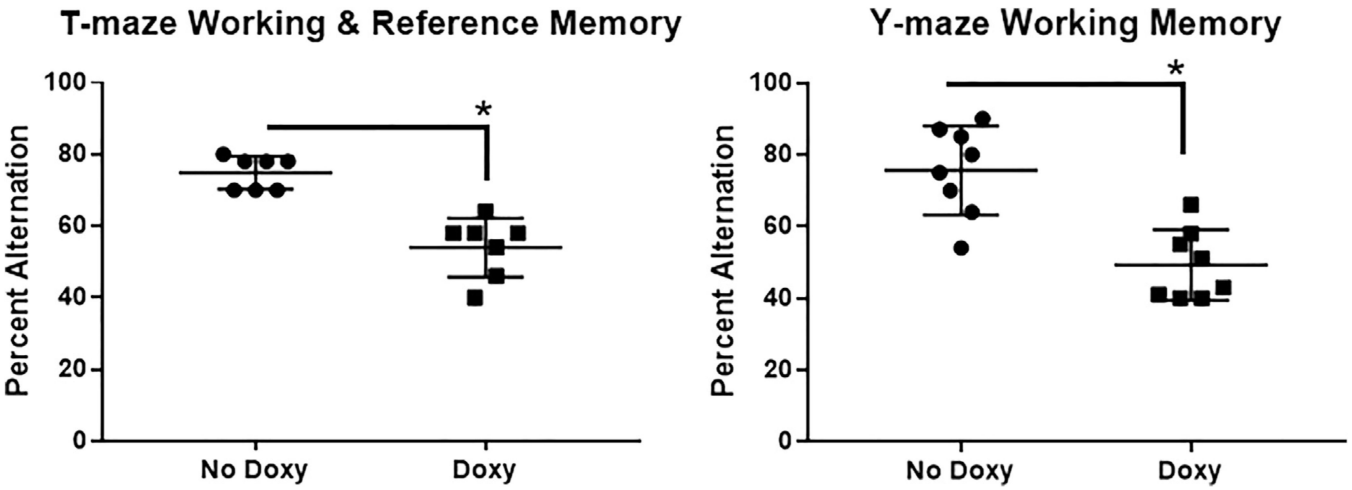

Fig. 3.

Cognitive impairment following doxycycline-induced miR-34a expression. A. On the forced alternation T-maze, a measure of working and reference memory, mice given Doxy were significantly impaired in their ability to successfully win-shift alternate (mean ± SEM percent successful alternations) [*t*-test: $t(14) = 4.719$, $p < 0.0005$]. B. On the spontaneous alternation Y-maze, a measure of working memory, mice given Doxy were significantly impaired in their ability to successfully undergo spontaneous alternation (mean ± SEM percent successful alternations) [*t*-test: $t(12) = 5.845$, $p < 0.0001$]. $N = 7–8$ mice/group. * $p < 0.05$.

Author Manuscript Author Manuscript Author Manuscript Author Manuscript

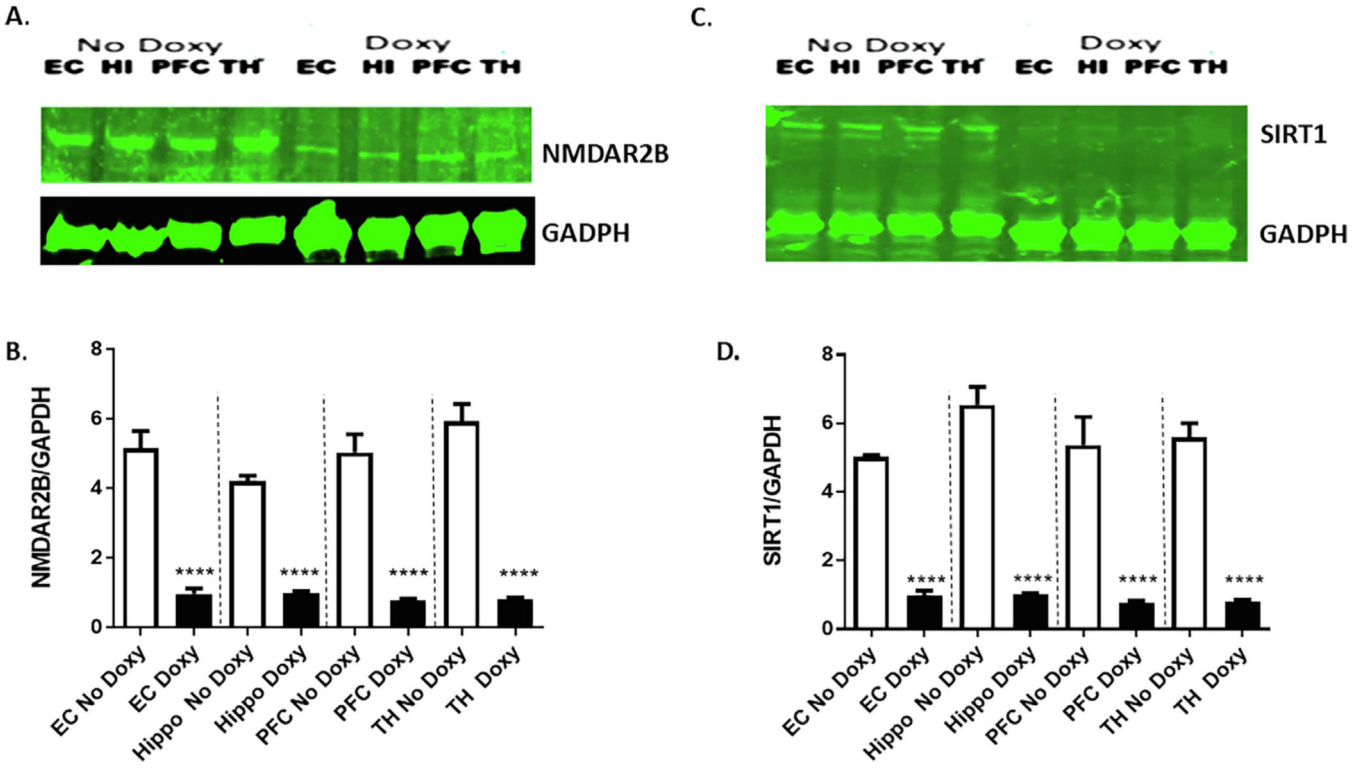

Fig. 4.

Suppression of miR-34a target proteins in doxycycline-induced miR-34a expression in brain regions of transgenic mice. A. Representative western blots of NMDAR-2B expression (GRIN2B antibody) among mice given Doxy (N = 3) vs No Doxy controls (N = 3) in the entorhinal cortex (EC), hippocampus (HI), prefrontal cortex (PFC), and thalamus (TH). B. Densitometric quantification of NMDAR-2B protein levels (normalized to GAPDH levels) is shown in the bar graph. Data are mean ± SEM, and the results shown are representative of three animals in each group. The significant Treatment main effect [$F(1,4) = 2381$, $p < 0.0001$] was followed up by taking a conservative approach to multiple comparison analyses within each brain region using the Bonferroni correction, **** $p < 0.0001$. C. Representative western blots of SIRT1 expression among mice given Doxy ($N = 3$) vs No Doxy controls (N = 3). D. Densitometric quantification of SIRT1 protein levels (normalized to GAPDH levels) is shown in the bar graph. Data are mean ± SEM, and the results shown are representative of three animals in each group. The significant Treatment main effect [$F(1,4) = 1003$, $p < 0.0001$] was followed up by taking a conservative approach to multiple comparison analyses within each brain region using the Bonferroni correction, **** $p < 0.0001$

Author Manuscript
Author Manuscript
Author Manuscript
Author Manuscript

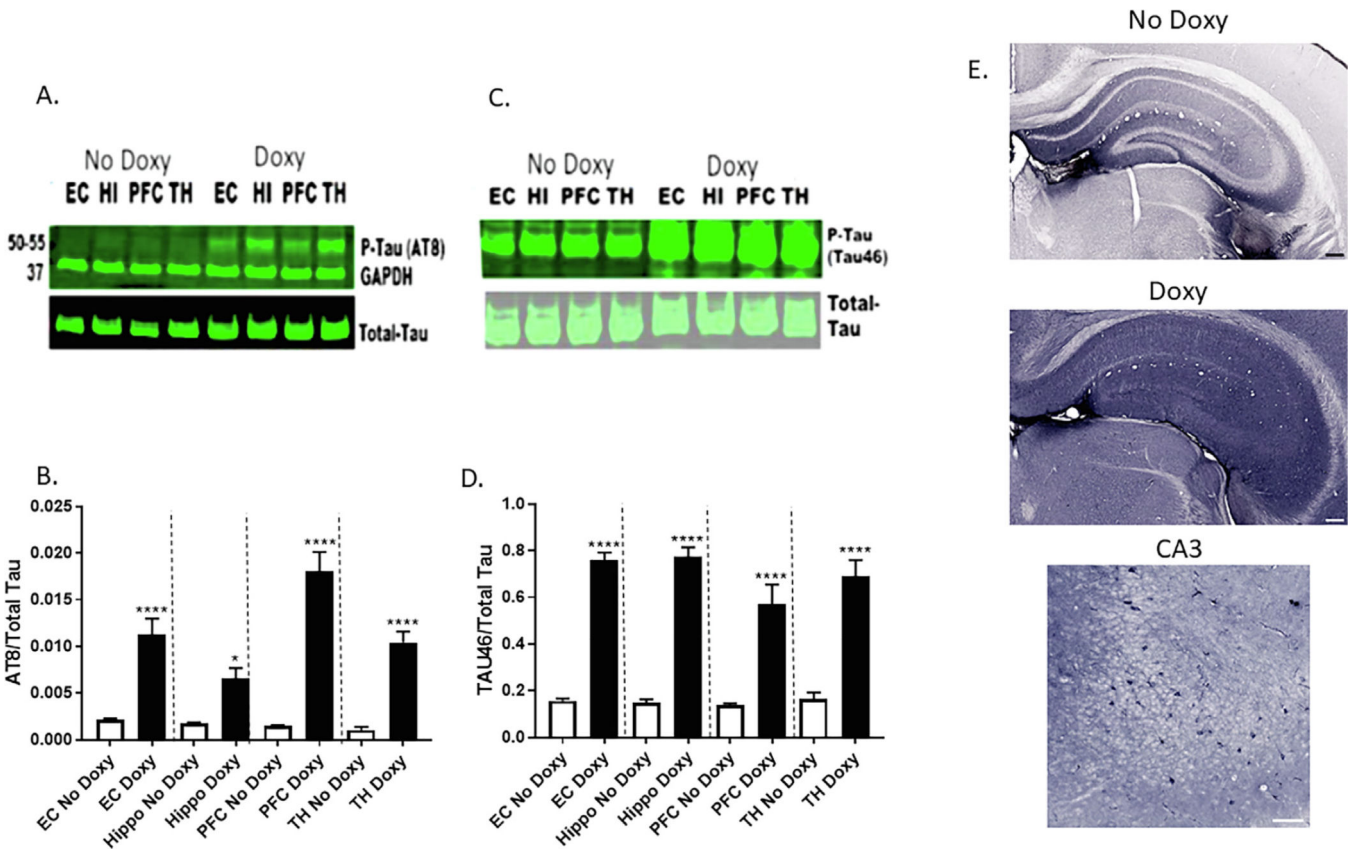

Fig. 5.

Upregulation of phosphorylation of Tau protein in doxycycline-induced miR-34a expression in brain regions of transgenic mice. A. Representative western blots of phospho-tau (AT8 antibody) expression among mice given Doxy vs No Doxy controls in the entorhinal cortex (EC), hippocampus (HI), prefrontal cortex (PFC), and thalamus (TH). B. Densitometric quantification of relative protein levels (p-Tau/total Tau) is shown in the bar graph. Data are mean ± SEM, and the results shown are representative of three animals in each group. The significant Treatment × Region interaction [$F(3,12) = 8.33$, $p < 0.005$] was followed up with Bonferroni-corrected multiple comparisons of the effect of Treatment in each brain region, * $p < 0.05$, **** $p < 0.0001$. C. Representative western blots of phospho-tau (Tau46 antibody) expression among mice given Doxy vs No Doxy controls. D. Densitometric quantification of respective protein levels (p-Tau/total Tau) is shown in the bar graph. Data are mean ± SEM, and the results shown are representative of three animals in each group. The significant Treatment main effect [$F(1,4) = 660.2$, $p < 0.0001$] was followed up with Bonferroni-corrected multiple comparisons of the effect of Treatment in each brain region, **** $p < 0.0001$. E. Expression of phosphorylated tau in the hippocampus of without (No (Doxy) over expressions of mir-34a, at low magnification (upper two panels; scale bars 200 μm), and high magnification with Doxy (lower panel; scale bar 100 μm).

Author Manuscript Author Manuscript Author Manuscript Author Manuscript

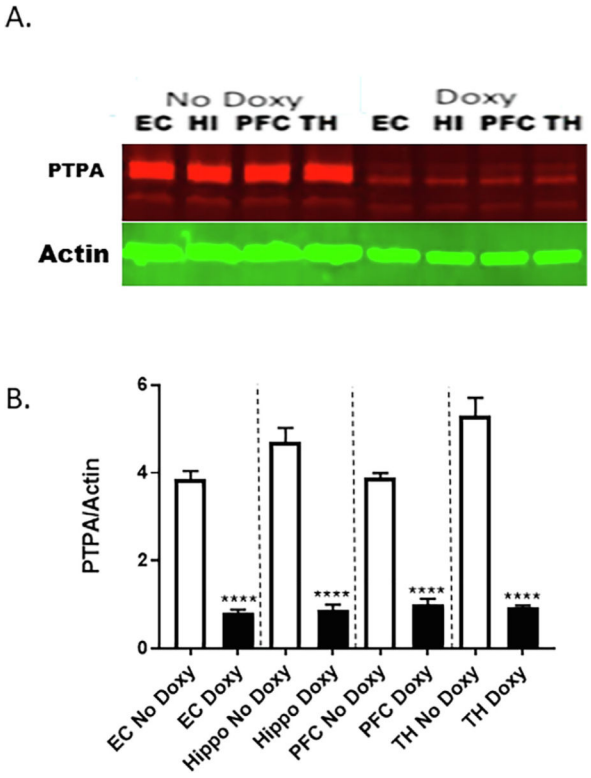

Fig. 6.

Suppression of PTPA protein in doxycycline-induced miR-34a expression in brain regions of transgenic mice. A. Representative western blots of PTPA expression among mice given Doxy vs No Doxy controls in the entorhinal cortex (EC), hippocampus (HI), prefrontal cortex (PFC), and thalamus (TH). B. Densitometric quantification of relative protein levels (PTPA/actin) is shown in the bar graph. Data are mean ± SEM, and the results shown are representative of three animals in each group. The significant Treatment × Region interaction [$F(3,12) = 12.51$, $p < 0.005$] was followed up with Bonferroni-corrected multiple comparisons of the effect of Treatment in each brain region, **** $p < 0.0001$.

Author Manuscript Author Manuscript Author Manuscript Author Manuscript

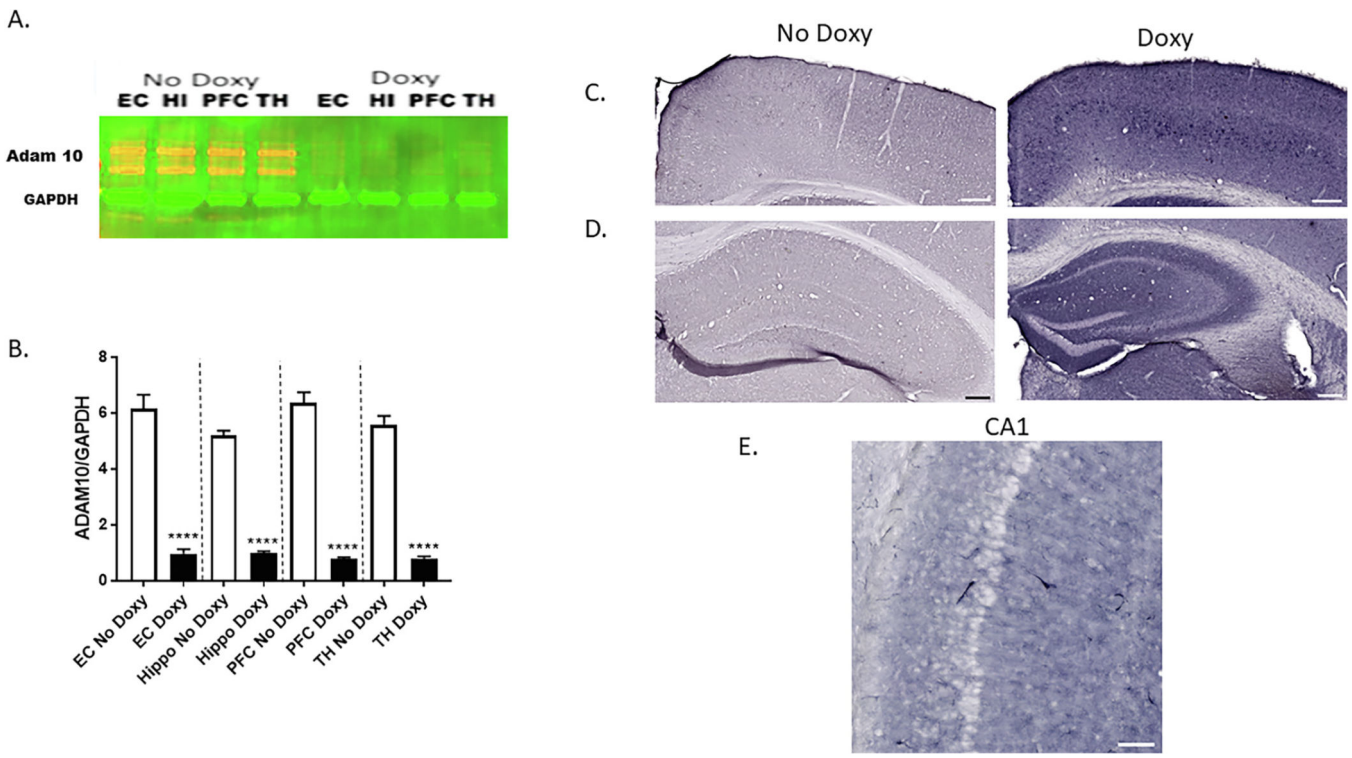

Fig. 7.

Downregulation of ADAM-10 in doxycycline-induced miR-34a expression in brain regions of transgenic mice. A. Representative western blots of Aβ expression (ADAM-10 antibody) among mice given Doxy vs No Doxy controls in the entorhinal cortex (EC), hippocampus (HI), prefrontal cortex (PFC), and thalamus (TH). B. Densitometric quantification of relative protein levels (ADAM10/GAPDH) is shown in the bar graph. Data are mean ± SD, and the results shown are representative of three animals in each group. The significant Treatment main effect [$F(1,4) = 820.6$, $p < 0.0001$] was followed up with Bonferroni-corrected multiple comparisons of the effect of Treatment in each brain region, **** $p < 0.0001$. Immunohistology of anti-β-amyloid antibody clone 6E10 in the cortex (C) and hippocampus (D) of mice given Doxy vs No Doxy controls. Scale bars 200 μm. E. High magnification of intracellular localization of anti-β-amyloid antibody clone 6E10 staining in the hippocampus. Scale bar 100 μm.

Author Manuscript Author Manuscript Author Manuscript Author Manuscript

Table 1

miR-34a Expression Levels in Brain (mean ± SEM fold change relative to No Doxy group).

	Cerebellum		Entorhinal Cortex		Hippocampus		Prefrontal Cortex		Temporal Cortex		Thalamus	
	Mean	**SEM**	**Mean**	**SEM**	**Mean**	**SEM**	**Mean**	**SEM**	**Mean**	**SEM**	**Mean**	**SEM**
No Doxy	1	0.12	1	0.18	1	0.07	1	0.115	1	0.16	1	0.14
Doxy	4635	2033	11,080	4485	3774	2187	4058	1844	5029	2861	3863	1985

Author Manuscript Author Manuscript Author Manuscript Author Manuscript

Table 2

miR-34a Target Gene Analysis.

Position 1086–1092 of Ppp2r4 3’ UTR mmu-miR-34a-5p	5’ … GGGCCUGCCCUUCUUCACUGCCC … ||||||| 3’ UGUUGGUCGAUUCUGUGACGGU
Position 1262–1268 of Ppp2r4 3’ UTR mmu-miR-34a-5p	5’ … CUUCCAGGGCCAGGCCACUGCCU … |||| ||||||| 3 ’ UGUUGGUCGAUUCU—GUGACGGU
Position 1170–1176 of Ppp2r4 3’ UTR hsa-miR-34a-5p	5’ …AGGCCUGCCCUUCUCCACUGCCC… ||||||| 3’ UGUUGGUCGAUUCUGUGACGGU
Position 377–383 of Adaml0 3’ UTR hsa-miR-34a-5p	5’ … AAUAUAUUUUUUUCAACUGCCAA… |||||| 3’ UGUUGGUCGAUUCUGUGACGGU
Position 1872–1878 of Adaml0 3’ UTR hsa-miR-34a-5p	5’ …UUUGGCAGGUACACACACUGCCC… ||||||| 3’ UGUUGGUCGAUUCUGUGACGGU
Position 37 6–382 of Adaml0 3’ UTR mmu-miR-34a-5p	5’ …AAUAUAUUUUUUUCAACUGCCAA… |||||| 3’ UGUUGGUCGAUUCUGUGACGGU
Position 838–844 of Sirt1 3’ UTR hsa-miR-34a-5p	5’ … UUCCACAAGUAUUAAACUGCCAA… |||||| 3’ UGUUGGUCGAUUCUGUGACGGU
Position 1381–1387 of Sirt1 3’ UTR hsa-miR-34a-5p	5’ …CCAGCUAGGACCAUUACUGCCAG… |||||| |||||| 3’ UGUUGGUCGAUUCUG----UGACGGU
Position 781–787 of Sirt1 3’ UTR mmu-miR-34a-5p	5’ … AUCUUCACCACAAAUACUGCCAA… |||||| 3’ UGUUGGUCGAUUCUGUGACGGU
Position 1277–1283 of Sirt1 3’ UTR mmu-miR-34a-5p	5’ … CCAGUUAGGACCAUUACUGCCAG… |||||| 3’ UGUUGGUCGAUUCUGUGACGGU
Position 7325–7331 of Grin2a 3’ UTR hsa-miR-34a-5p	5’ … AUGCCCCUGAGCACA--CACUGCCU… ||| |||||| 3’ UGUUGGUCGAUUCUGUGACGGU
Position 7005–7011 of Grin2a 3’ UTR mmu-miR-34a-5p	5’ … ACAUACAUAUGCACACACUGCCU… ||||||| 3’ UGUUGGUCGAUUCUGUGACGGU
Position 1682–1688 of GRIN2B 3’ UTR hsa-miR-34a-5p	5’ …GAAAUGAAUAUGUAUCACUGCCG… ||||||| 3’ UGUUGGUCGAUUCUGUGACGGU
Position 3279–3285 of GRIN2B 3’ UTR hsa-miR-34a-5p	5’ …UGCCUUGUCCUCAUUACUGCCAU… |||||| 3’ UGUUGGUCGAUUCUGUGACGGU

Author Manuscript Author Manuscript Author Manuscript Author Manuscript

Position 1674–1680 of Grin2b 3' UTR mmu-miR-34a-5p	5'	…GAAAUGAAUAUUUGUCACUGCCC…
		||||||
	3'	UGUUGGUCGAUUCUGUGUGACGGU
Position 3293–3299 of Grin2b 3' UTR mmu-miR-34a-5p	5'	… UACCUUGUUCUUGUUACUGCCAU…
		|||||
	3'	UGUUGGUCGAUUCUGUGUGACGGU
Position 10723–10729 of Grin2b 3' UTR mmu-miR-34a-5p	5'	…GUUUGUGUAUUUUACCACUGCCC…
		||||||
	3'	UGUUGGUCGAUUCUGUGUGACGGU
Position 13064–13070 of Grin2b 3' UTR mmu-miR-34a-5p	5'	…UCUUCGUCUUUCAGCU---CACUGCCU…
		||||| ||||||
	3'	UGUUGGUCGAUUCUGUGUGACGGU